A Comparative Study of Mesospheric Zonal Wind Observations from Na Lidar and Multistatic Meteor Radars above Hefei, China

Chao Ban[1,2], Xin Fang[3], Wen Yi[3,4,5], Jie Zeng[3,4,5], Gunter Stober[6], Weilin Pan[1,2,7], Tao Li[3,4], and Xianghui Xue[3,4,5]

[1]State Key Laboratory of Atmospheric Environment and Extreme Meteorology, Institute of Atmospheric Physics, Chinese Academy of Sciences, Beijing, China
[2]Laboratory of Middle Atmosphere and Global Environment Observation, Institute of Atmospheric Physics, Chinese Academy of Sciences, Beijing, China
[3]CAS Key Laboratory of Geospace Environment, School of Earth and Space Sciences, University of Science and Technology of China, Hefei, China
[4]CAS Center for Excellence in Comparative Planetology, University of Science and Technology of China, Hefei, China
[5]Anhui Mengcheng National Geophysical Observatory and Research Station, School of Earth and Space Sciences, University of Science and Technology of China, Hefei, China
[6]Institute of Applied Physics and Oeschger Center for Climate Change Research, Microwave Physics, University of Bern, Bern, Switzerland
[7]University of Chinese Academy of Sciences, Beijing, China

Correspondence to: Xin Fang (xinf@ustc.edu.com), Wen Yi (yiwen@ustc.edu.com)

Abstract. This study compares zonal wind measurements from a Na lidar at the University of Science and Technology of China (USTC) with those from the multistatic meteor radar system near Hefei, China. The meteor radar data used for comparison with the lidar include three sources: Mengcheng Meteor Radar (MCMR), Changfeng remote Receiver (CFR), and wind derived closer to the lidar beam using the Volume Velocity Processing (VVP) method. ~~Simultaneous hourly observations over 34 nights from 2022 to 2023, spanning about 300 hours between 82 and 98 km, were analyzed.~~ About 300 hours of simultaneous, coincident observations from meteor radars and a Na lidar over 34 nights during 2022–2023, covering altitudes from 82 to 98 km, were analyzed. The parameters of zonal wind between lidar and meteor radar such as correlation coefficients, zonal wind mean, variance and zonal wind different are presented. Both monostatic meteor radar (MCMR and CFR) and multistatic meteor radars (VVP) zonal winds show good consistency with lidar zonal winds. Compared with monostatic radars, VVP zonal winds exhibit better agreement with the lidar above 90 km, both in zonal wind variance and radar-to-lidar zonal wind ratio. These results demonstrate that the VVP method provides a reliable approach for retrieving meteor radar winds and can improve wind estimates in the 90–98 km region.

1 Introduction

Investigating upper atmospheric dynamics is essential for understanding global circulation patterns, energy transfer processes, and the lower and upper atmosphere coupling. The mesosphere and lower thermosphere (MLT) region, situated approximately 70-110 km above the Earth's surface, plays an important role due to its intricate interactions with the stratosphere and the thermosphere (Smith, 2012). Wind measurements in this region provide essential insights into the atmospheric tides, gravity waves, and planetary waves that drive these interactions (Fritts & Alexander, 2003).

Na lidar and meteor radar are two essential remote sensing techniques for measuring winds in the MLT region. Na lidars utilize the resonance fluorescence of Na atoms present in a layer between 80-105 km altitude to provide high-resolution measurements of temperature, Na density, and wind velocity (She and Yu, 1994). The ability of Na lidar systems to provide precise vertical profiles of wind and temperature with high temporal resolution makes them invaluable for studying turbulence (Guo et al., 2017) and gravity wave dynamics (Hu et al., 2002; Ban et al., 2015; Cao et al., 2016; Yuan et al., 2016), vertical fluxes (Gardner and Liu, 2007; Chu et al., 2022; Li et al., 2022) and atmospheric instability (Bishop et al., 2004; Yue et al., 2010). Meanwhile, the Na lidar is suitable for tidal analysis (She et al., 2004; Yuan et al., 2006) and long-term trend research (She et al., 2015).

Meteor radars, on the other hand, detect the reflection of radio waves from the ionized trails left by meteoroids entering the Earth's atmosphere (Hocking et al., 2001; Holdsworth et al., 2004). These reflections, typically observed at altitudes between 80 and 100 km, provide indirect measurements of wind velocities through Doppler shift analysis. Unlike Na lidar, which mainly operates in clear-sky weather, meteor radar is insensitive to weather conditions, resulting in significantly higher observation time coverage. However, the temporal and vertical resolution of wind inversion achieved by meteor radar is lower than that of Na lidar. Typically, it employs a time resolution of 1 hour with a vertical resolution of 2 km or 2 hours with a vertical resolution of 3 km, primarily determined by the number of meteors. In addition, the horizontal averaging range of meteor radar wind is nearly circular region, with a radius of 200 km (Liu et al., 2017). These features make the meteor radar well-suited for capturing large-scale wave dynamics (Chau et al., 2017; Yang et al., 2023) and conducting long-term climatological studies (Kishore & Hocking, 2010; Yi et al., 2019; Hindley et al., 2022) in the MLT region.

Recently, multistatic meteor radar observations, combined with 3DVAR (Stober et al., 2021, 2022) or NDVVP (newly developed volume velocity processing, VVP is used here for simplicity) (Zeng et al., 2024) methods, have enabled the retrieval of the horizontal distribution of winds in MLT region. Both methods can derive wind vectors from multi-directional radial velocity measurements. The 3DVAR method is primarily based on griding, optimal estimation, and Bayesian statistics, whereas the NDVVP method assumes linear winds within observation regions and applies WGS84 coordinate system and several iterations. Compared with traditional meteor radar retrieval methods, both the 3DVAR and NDVVP method can provide wind estimates at any individual location within the observation domain, thereby reducing the influence of large-scale horizontal averaging on the results.

Previous comparisons between the wind observation by Na lidar and meteor radar have been reported. For example, simultaneous wind observations from Na lidar and meteor radar were compared at Starfire Optical Range, New Mexico (SOR, NM, 35° N, 106.5° W) (Liu et al., 2002). The authors found that the correlation coefficients of the two instruments varied between 0.63 and 0.70 for the wind at 86 and 93 km, and the correlation coefficients varied from 0.94 to 0.95 when comparing the averaged variations over the night, indicating the large-scale process was effectively captured by both instruments. Further comparative work (Frank et al., 2005) conducted in Maui, Hawaii (20.75° N, 156.43° W) found a better correlation, with coefficients of 0.89 and 0.91 for zonal wind and meridional wind, respectively. Recently, Qiao et al. (2025) reported observations from the Chilean Observation Network De MeteOr Radars (CONDOR) and compared horizontal wind with Na lidar data at the Andes Lidar Observatory (ALO, 30.25° S, 71.00° W). They found the zonal and meridional wind correlation coefficients are 0.79 and 0.75, respectively, with the ALO Na lidar winds are larger than those measured by meteor radar.

In this study, we compare the zonal wind measurements from Na lidar with the point-to-point observations from both monostatic meteor radars (MCMR and CFR) and multistatic meteor radar (VVP). Only time periods during which all instruments were simultaneously operating were selected, resulting in approximately 300 hours of coincident measurements. Additionally, the paper presents a summary of the Na lidar and meteor radar comparison results at various stations. Detailed descriptions of instruments and datasets are provided in Section 2, followed by the comparison results in Section 3 and a discussion in Section 4. Finally, a summary is presented in Section 5.

2 Instruments and Data Sets

The USTC Na lidar used in this study is a narrowband system that simultaneously measures nighttime Na density, wind, and temperature in the MLT region, having made observations since January 2012 (Li et al., 2012). To detect the zonal momentum and heat fluxes of gravity waves (Li et al., 2022), the lidar employs three beams with three telescopes directed eastward, westward, and zenith direction, making the system detect only zonal wind. The lidar's final beam has a full divergence angle of 0.7–0.8 mrad, resulting in an average wind measurement region with a circular diameter of approximately 80 meters at 90 km. The typical data temporal resolution of this Na lidar is 15 minutes. For comparison with meteor radar, we retrieve zonal wind with a temporal resolution of 1 hour. The zonal wind uncertainties for resolutions of 1 hour and 2 km ~~resolutions~~ range from 3.0 m/s at 92 km to 7.5 m/s at 82 km and 102 km. In this study, the zonal winds with uncertainties larger than 10 m/s are excluded.

The Mengcheng Meteor radar (MCMR, 33.36°N, 116.45°E) is a traditional meteor radar operating at a frequency of 38.9 MHz with a peak power of 24 kW, starting observations from April 2014 (Yi et al., 2023), which belongs to the meteor detection radar (MDR) series manufactured by ATRAD and is similar to the Buckland Park meteor radar system described by Holdsworth et al. (2004). The Changfeng remote receiver (CFR, 31.92° N, 117.21° E), operational since January 2022, can receive the forward scattering signal from the Mengcheng transmitter synchronously. To permit accurate range and

Doppler estimates at the remote site, the system timing, frequency, and clocks at both sites are synchronized with GPS-disciplined oscillators (GPSDOs) (Spargo et al., 2019). ~~The Mengcheng Meteor radar (MCMR, 33.36°N, 116.45°E) is a traditional meteor radar operating at a frequency of 38.9 MHz with a peak power of 24 kW, starting observations from April 2014 (Yi et al., 2023). The Changfeng remote receiver (CFR, 31.92° N, 117.21° E), operational since January 2022, can receive the forward scattering signal from the Mengcheng transmitter synchronously.~~ The VVP zonal winds were obtained from the combined multistatic meteor radar data, including MCMR, CFR and the Wuhan meteor radar. For comparison with the lidar, VVP winds at the grid point closer to the lidar beam were selected. Detailed descriptions of the multistatic meteor radar systems have been reported by previous work (Zeng et al., 2024). The meteor radar zonal wind temporal and vertical resolutions used in this study are also 1 hour and 2 km, respectively, consistent with those of the Na lidar. Zonal winds were estimated only when at least six meteor echoes were available within a 1-hour and 2-km time-height bin, resulting in zonal wind uncertainties of less than 10 m/s over the altitude range of 80-100 km.

Figure 1a shows the geographic locations of the Na lidar and meteor radar. The distances between Na lidar and MCMR and between Na lidar and CFR are 181 km and 17 km, respectively. The dots in Figure 1a, 1b, 1c, and 1d are meteor detections by MCMR and CFR at 00:00 UT, 06:00 UT, 12:00 UT and 18:00 UT on 17-19, July, 2023. Both the backscattered echoes from MCMR and the forward scattered echoes from CFR are observed within roughly circular regions with radius of 200–300 km, with the CFR's echo region being slightly larger. The meteor radar detects more meteors around dawn (Figure 1a and 1d) than around dusk (Figure 1c), and the number of detections at all times is sufficient for reliable wind retrieval. The total number of meteor detections at CFR is about 89% of the observations of MCMR, consistent with previous study (Stober & Chau, 2015). Figure 1e presents the histogram of normalized meteor numbers versus distance observed by MCMR, showing backscattered echoes within a circular region of approximately 220 km radius, mainly concentrated 60–180 km from the MCMR receiver. In contrast, Figure 1f shows that the forward-scattered echoes observed by CFR are more widely and evenly distributed, covering a circular region with a radius of 300 km and mainly concentrated 60–220 km from the CFR.

This study uses 34 nights (~300 hours) of simultaneous zonal wind observations conducted between January 2022 and December 2023 to compare zonal wind measurements from the three instruments mentioned above. It is well known that the detection accuracy of Na lidar and meteor radar depends on the sodium density and the number of meteors, respectively. Figure 2a shows the distributions of the Na density from Na lidar and hourly meteor counts from meteor radars. Note that the meteor counts represent the total number between 10:00 and 22:00 UT, averaged from the meteor radar observation from 2022 to 2023. The vertical profiles of Na density and meteor counts both exhibit Gaussian distributions. The peak Na density occurs at 92.29 km, with a peak density of 2700 cm^{-3}, consistent with previous long-term observations in Hefei (Li et al., 2018). The peak altitudes for the MCMR and CFR meteor counts are 89.97 km and 91.10 km, with peak count of 1000 and 1050 per night, respectively. Notably, the maximum signal altitude of the Na lidar is approximately 1 km and 2 km higher than that of CFR and MCMR, respectively. The peak altitude of CFR detection ~~altitude~~ is 1 km higher than that of~~the~~ MCMR, primarily caused by the forward scattering geometry (Stober & Chau, 2015), with lower equivalent frequencies

show a peak at approximately 37.5 MHz, which is 1.4 MHz lower than the Mengcheng transmitted frequency (38.9 MHz). Based on the height distributions of Na density and meteor counts, zonal wind measurements between 82 and 98 km are selected for comparison in this study. Figure 2b depicts the meteor counts from the two stations with UT hour, clearly showing that the meteor counts increase from ~300 count/hour to ~1300 count/hour with time from 12:00 UT to 22:00 UT. Notably, the meteor counts of CFR are more than that of MCMR between 18:00 and 21:00 UT.

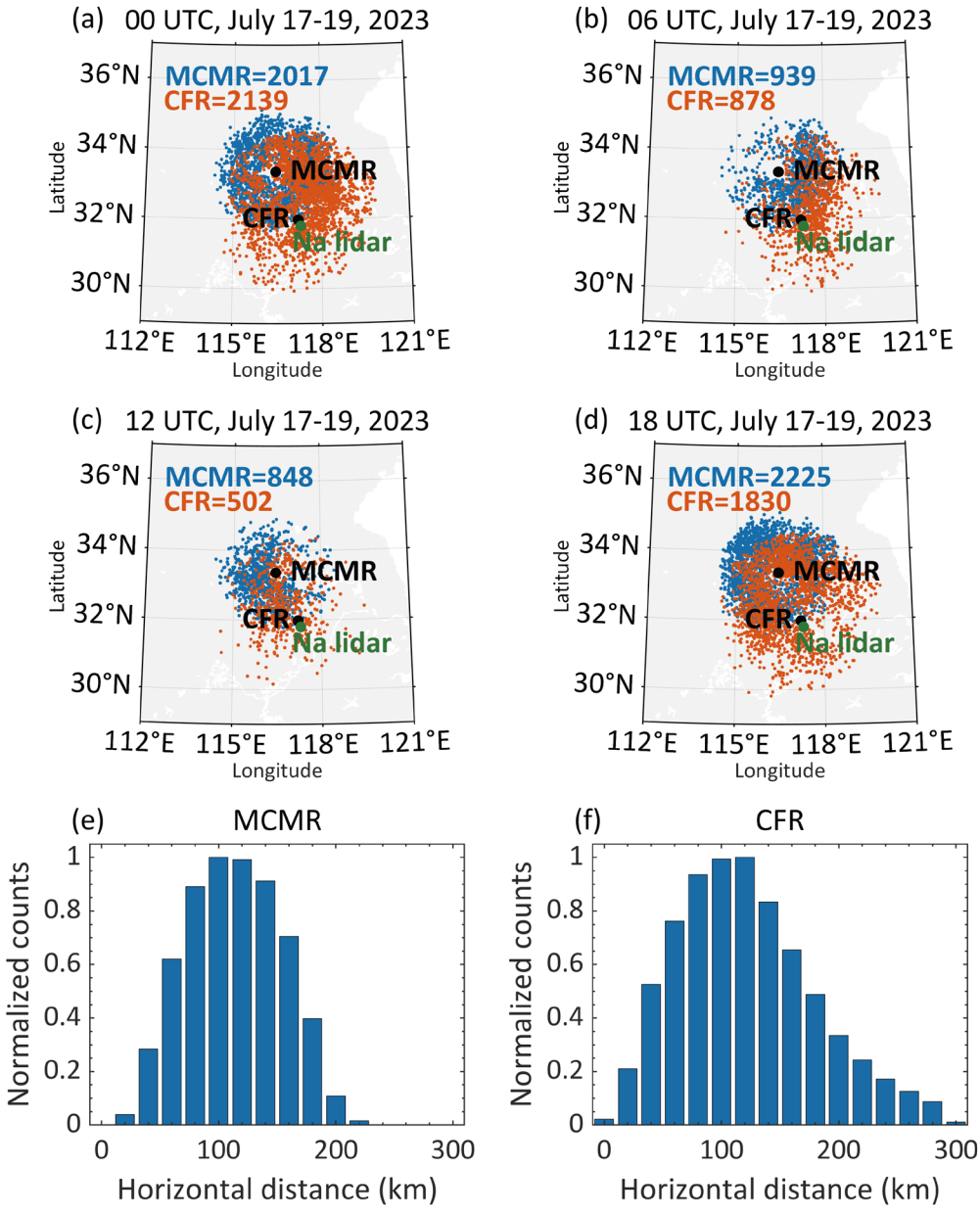

135 **Figure 1.** Meteor detections observed by Mengcheng meteor radar (blue dots) and Changfeng receiver (orange dots) at 00:00 UT (**a**), 06:00 UT (**b**), 12:00 UT (**c**), and 18:00 UT (**d**) on 17-19, July, 2023. Geographic locations of Na Lidar (green circle), Mengcheng meteor radar and Changfeng remote receiver (black circles) are also shown. Histograms of normalized meteor number versus distance observed by the Mengcheng (**e**) and Changfeng (**f**) receivers. The distance represents the horizontal distance from the meteor echoes to receivers.

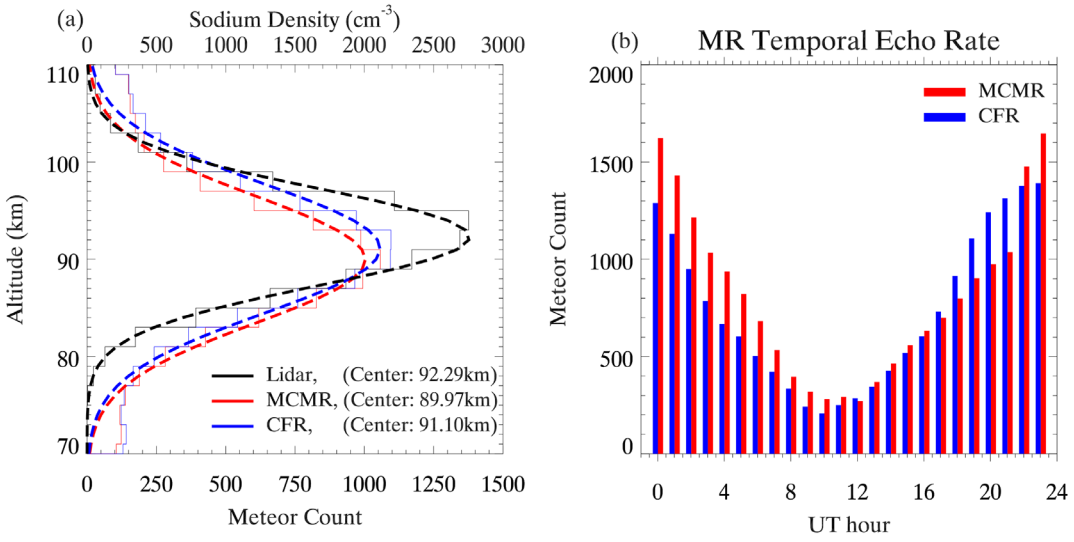

Figure 2. (**a**) Height distributions of the Na density from Na lidar and meteor counts from meteor radars (solid lines in 2km bins). The curves fitted to the density number (black dashed line) and meteor counts (red dashed line for MCMR and blue dashed line for CFR) assuming a Gaussian distribution. (**b**) Hourly detected meteor counts, the red bars present MCMR and the blue bars present CFR.

3 Comparison

Figure 3 demonstrates the zonal wind observations from (a) Na lidar, (b) MCMR, (c) CFR, and (d) VVP between 12:00 and 21:00 UT on February 25, 2023. The measurements exhibit good consistency in their overall temporal and vertical variations. ~~Figures 3a, 3b, 3c, and 3d display zonal wind observations from the Na lidar, MCMR, CFR, and VVP between 12:00 and 21:00 UT on February 26, 2023. The four results demonstrate good consistency in their overall structure.~~ For example, the zonal wind during this night is predominantly eastward with the maximum wind of 70 m/s at 15:00 UT around 96 km. This peak in zonal wind shows a downward progression over time, with a second maximum occurring at 21:00 UT around 93 km. The zonal wind appears modulated by a wave of 5-6 hours, as evidenced by the minimum zonal winds observed at 13:00-14:00 and 19:00 UT around 90 km. However, there are differences in altitude coverage among the four results. In Figure 3a, the Na lidar's zonal wind observations cover altitudes from 80 km to 100 km at 12:00 UT, with the detection range gradually narrowing over time; by 17:00 UT, the lower limit of zonal wind measurement is 84 km due to decreasing Na density, which increases the zonal wind uncertainty. In contrast, the meteor radars initially cover a detection range of 82 to 96 km at 12:00 UT, limited by lower meteor counts (Figure 2b). As the meteor counts increase with time between 12:00 and 21:00 UT (Figure 2b), the detection range of the meteor radars expands. The VVP zonal winds exhibit broader temporal and vertical coverage, which may result from the inclusion of observations from multiple stations. Figure 4 compares vertical profiles at different times for the Na lidar and meteor radars, revealing that the zonal winds observed by the Na lidar and VVP exhibit more variation in their vertical profiles than the zonal winds observed by MCMR and CFR. For instance, the Na lidar and

VVP zonal wind profiles at 12:00, 16:00, and 20:00 UT demonstrate stronger wave perturbations than those from the monostatic meteor radars. It should be noted that the VVP zonal wind at 100 km exhibits unusual variability (e.tg., at 14:00 UT, 15:00 UT, and 20:00 UT). To avoid potential biases from these anomalous values, only data at altitudes no higher than 98 km were used for comparison.

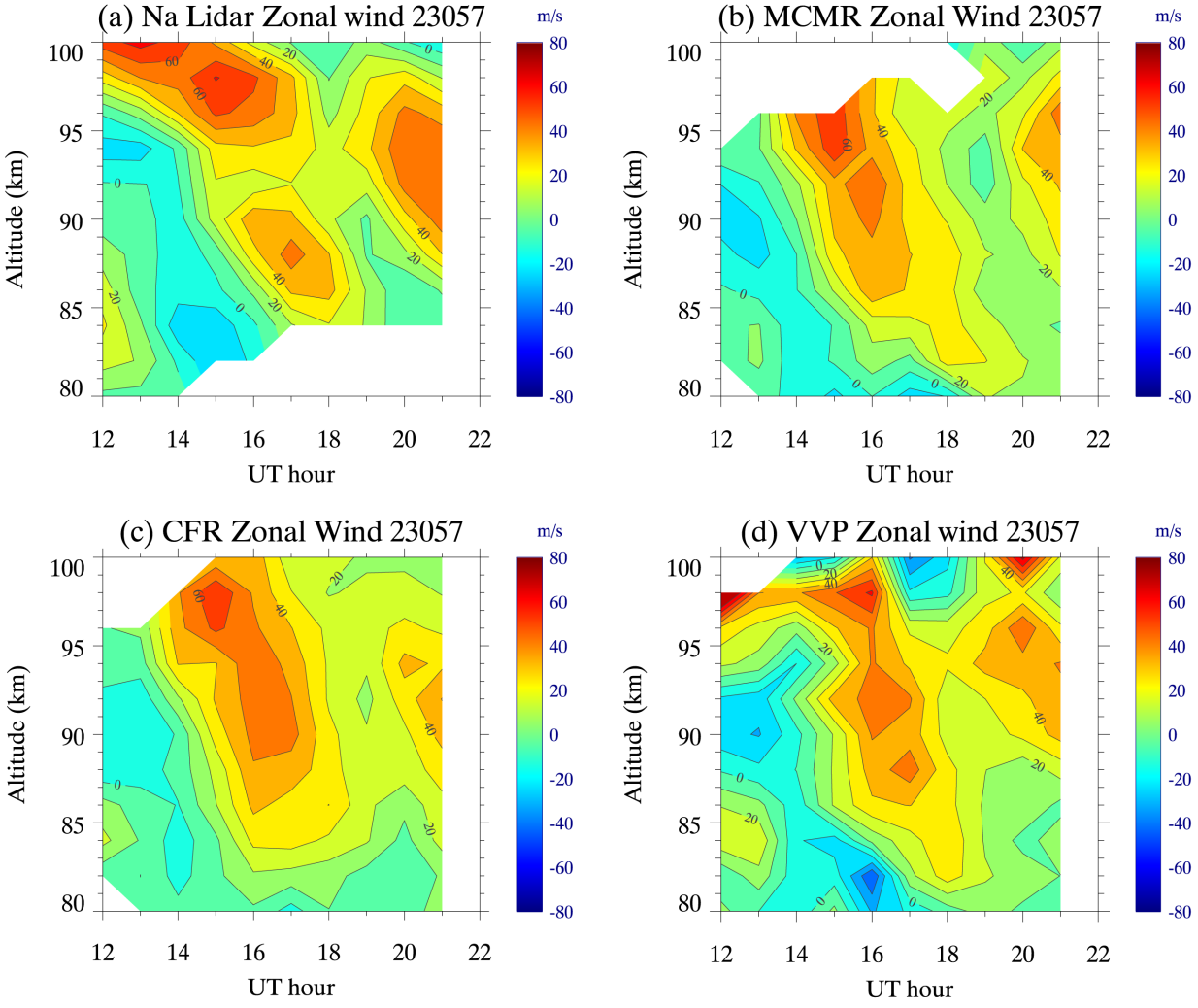

Figure 3. Zonal wind measurements from Na lidar (**a**), Mengcheng meteor radar (**b**), Changfeng receiver (**c**), and VVP (**d**) between 12:00 and 21:00 UT, 26 February 2023.

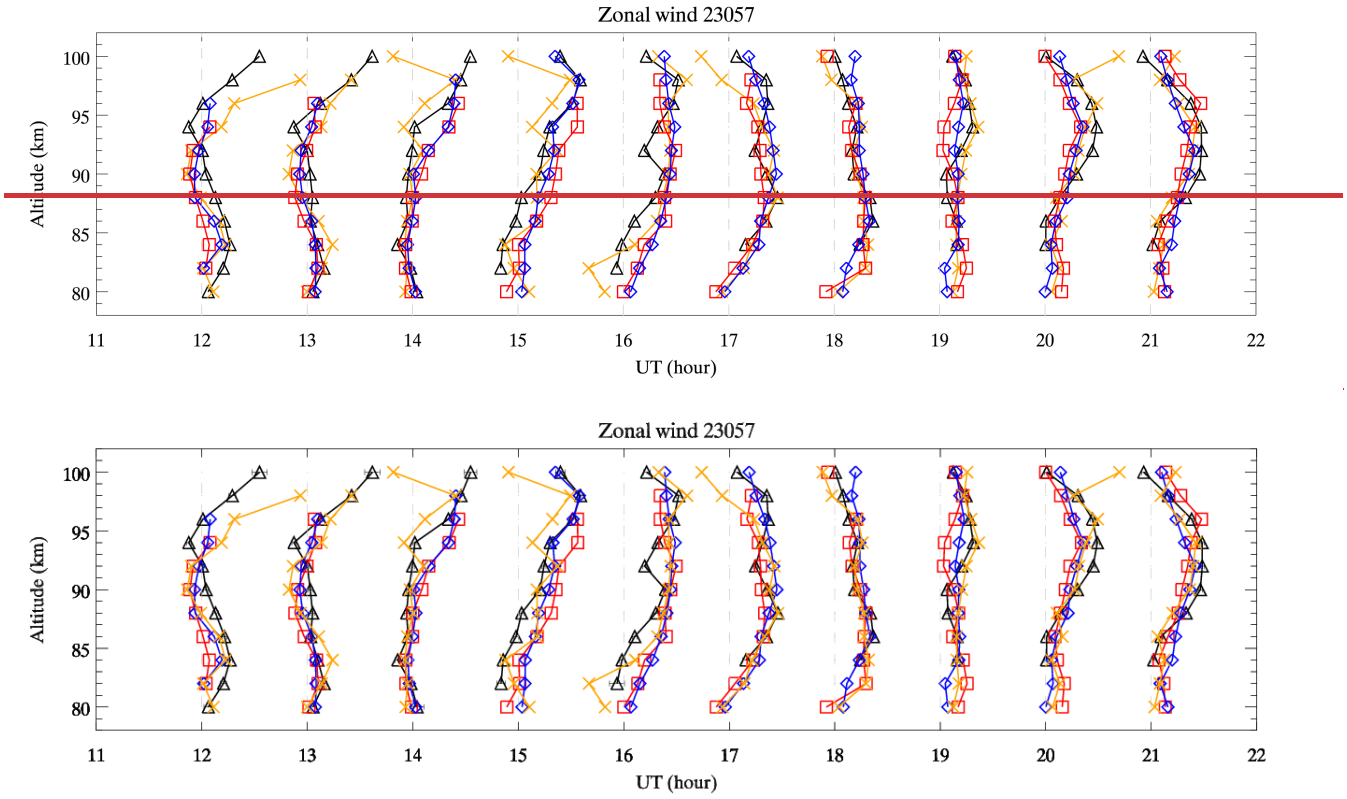

Figure 4. Zonal wind vertical profiles during the night of 26 February 2023. Na lidar, MCMR, CFR, and VVP profiles are marked with black triangles, red squares, blue diamonds, and orange cross, respectively. The black error bars indicate the uncertainties of the Na lidar zonal wind. The horizontal distance between each vertical lines corresponds to 120 m/s.

The zonal wind histograms for the Na lidar and meteor radars are presented in Figure 5. These histograms generally exhibit ~~a~~ Gaussian distributions. The statistical and Gaussian fit parameters are listed in Table 1. According to Table 1, there are 2,216 coincident samples in this study. The mean zonal winds from lidar and meteor radars are 15.13 m/s (Na lidar), 14.25 m/s (MCMR), 15.96 m/s (CFR), and 15.57 m/s (VVP), aligning closely with the center wind of the Gaussian fits, indicating that the mean zonal winds from the lidar and radars are generally consistent. The variance of the lidar zonal wind (1857 m^2/s^2) is 56%, 95%, and 33% larger than that of MCMR (1192 m^2/s^2), CFR (951 m^2/s^2), VVP (1398 m^2/s^2), respectively, illustrating that the zonal wind perturbations measured by the lidar are greater than those observed by the radars. The Gaussian fit standard deviations (STD) of Na lidar, MCMR, CFR, and VVP are 46.22 m/s, 37.25 m/s, 32.51 m/s, and 38.90 m/s, respectively.

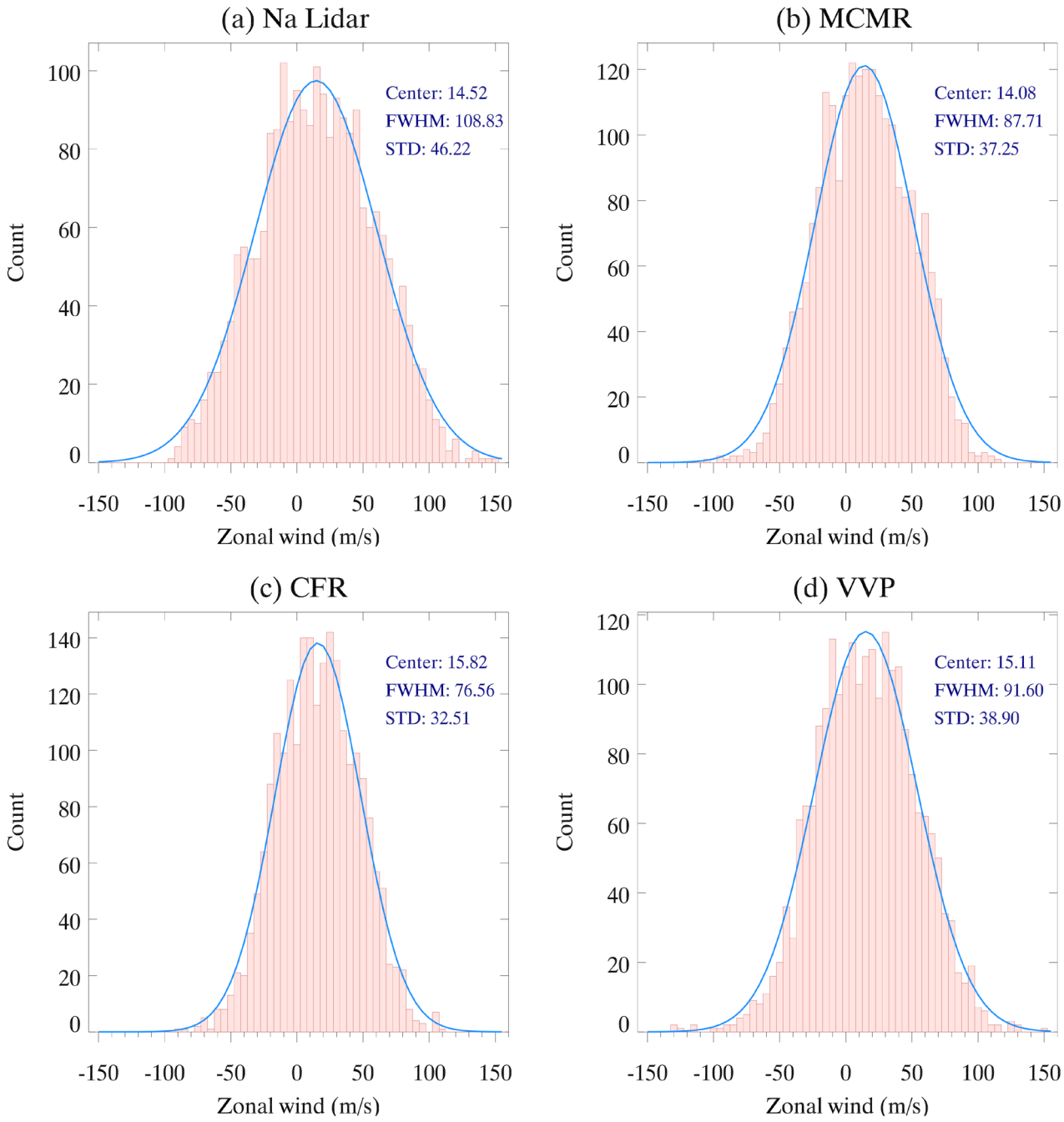

Figure 5. Histograms of zonal wind from Na Lidar (**a**), MCMR (**b**), CFR (**c**), and VVP (**d**). The curve fitted to the zonal wind (blue solid line) assuming a Gaussian distribution. The Gaussian fit parameters are presented.

Parameter	Na Lidar	MCMR	CFR	VVP
Sample number		2216		
$< u > (m/s)$	15.13	14.25	15.96	15.57
$Var[u]\ (m^2/s^2)$	1857	1192	951	1398
Gaussian fit center $< u > (m/s)$	14.52	14.08	15.82	15.11
Gaussian fit STD$[u]\ (m/s)$	46.22	37.25	32.51	38.90

Table 1. Statistical and Gaussian fit parameters for zonal wind measurements from Na lidar and meteor radars.

Scatter plots of zonal wind between 82 and 98 km, observed by the Na lidar compared to the MCMR, CFR, and VVP, are shown in Figures 6a, 6b, and 6c. The correlation coefficients for lidar-MCMR, lidar-CFR, and lidar-VVP are 0.85, 0.82, and 0.80, respectively. Figure 7 presents the histograms of the differences in zonal wind between the lidar and the radars. These differences generally follow a Gaussian distribution, with center values of 0.43 m/s for lidar-MCMR, -0.90 m/s for lidar-CFR and -0.50 m/s for lidar-VVP. The large~~high~~ correlation coefficients and small differences indicate that the zonal wind measurements from the Na lidar and meteor radars are generally consistent. However, the zonal wind from the Na lidar is greater than that from the meteor radars, as illustrated in Figure 6. The slopes of the linear fits are 0.80, 0.72, and 0.87 for lidar-MCMR, lidar-CFR, and lidar-VVP, implying that the zonal wind measured by the lidar is 1.25, 1.39, and 1.15 times that of the MCMR, CFR, and VVP, respectively. The statistical and Gaussian fit parameters of the combined dataset are summarized in Table 2. The medians of the differences between the lidar and radars are 0.52 m/s for lidar-MCMR, -0.73 m/s for lidar-CFR, and -0.13 m/s for lidar-VVP, which are similar to the Gaussian fit center values. Among the meteor radar zonal winds, the VVP winds have the smallest lidar/radar wind ratio (1.15) and the smallest median wind difference (-0.13 m/s), indicating better agreement with the lidar measurements.

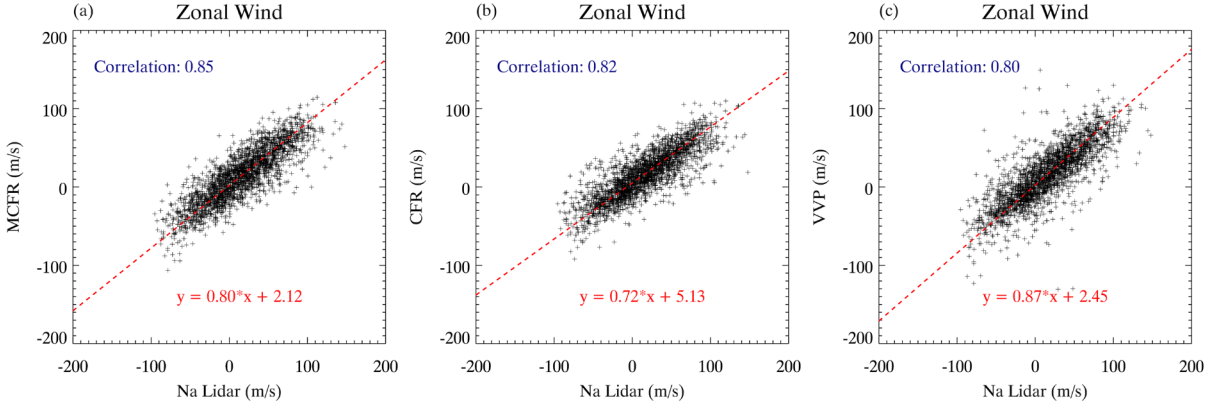

Figure 6. Scatter plots and linear fits for lidar versus MCMR (**a**), lidar versus CFR (**b**), and lidar versus VVP (**c**), using all coincident measurements within the 82-98 km altitude range.

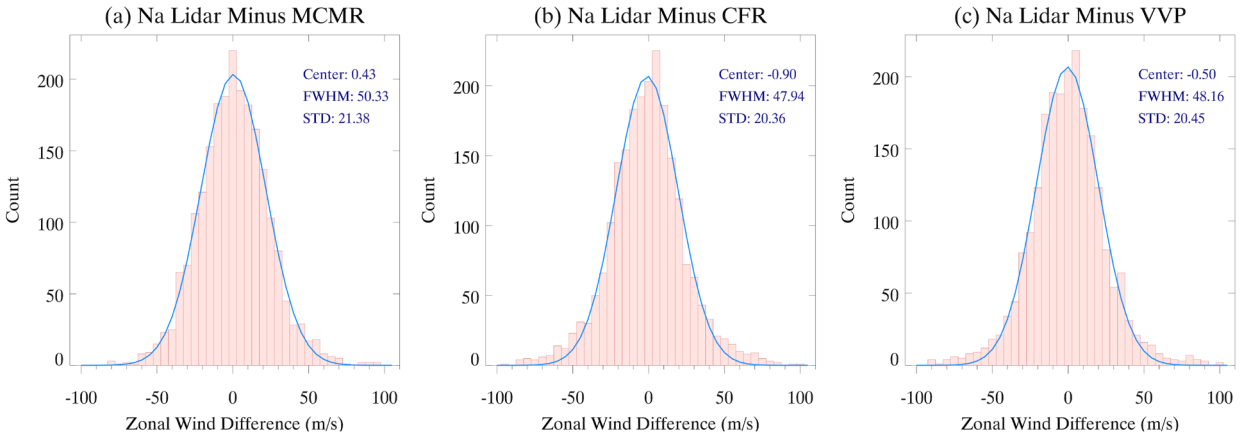

Figure 7. Histograms of zonal wind difference from Na Lidar-MCMR (**a**), lidar-CFR (**b**), lidar-VVP (**c**). The curve fitted to the zonal wind difference (blue solid line) assuming a Gaussian distribution. The Gaussian fit parameters are presented.

Parameter	Lidar-MCMR	Lidar-CFR	Lidar-VVP
$Correlation\ coefficient$	0.85	0.82	0.80
$Median[u_{Lidar} - u_{MR}]\ (m/s)$	0.52	-0.73	-0.13
$Median[\lvert u_{Lidar} - u_{MR}\rvert]\ (m/s)$	14.55	14.38	14.43
$STD[u_{LIDAR} - u_{MR}]\ (m/s)$	23.03	24.82	25.82
$Gaussian\ fit\ center\ [u_{Lidar} - u_{MR}]\ \ (m/s)$	0.43	-0.90	-0.50
$Gaussian\ fit\ STD[u_{Lidar} - u_{MR}](m/s)$	21.38	20.36	20.45

Table 2. Statistical and Gaussian fit parameters for zonal wind difference from lidar-MCMR, lidar-CFR, and lidar-VVP.

The comparison described above includes data from all altitudes between 82 and 98 km. The altitude dependence of this comparison is illustrated in Figure 8. Figure 8a presents the correlation coefficients for zonal wind measurements from the lidar and radars at different altitudes. The maximum coefficient, approximately 0.9, occurs between 86 and 92 km, corresponding to the altitudes of the highest sodium density and the greatest number of meteors, as shown in Figure 2a. The correlation coefficients decrease at 82 km and 98 km due to reduced signals resulting from lower sodium density and fewer meteors at these altitudes. However, the coefficients at these levels remain greater than 0.5.

Figure 8b displays the zonal wind variance for the Na lidar and meteor radars across different altitudes. The lidar and radar variances increase with altitude, consistent with the fact that upward-propagating wave amplitudes increase as air density decreases. The zonal wind variance for the lidar is 1100 m^2/s^2 at 82 km, increasing to 1900 m^2/s^2 at 88 km, and then stabilizing at this level between 88 and 94 km, before rising to 2500 m^2/s^2 at 98 km. Furthermore, Figure 8b demonstrates that the lidar zonal wind variance is greater than that of the radars at all altitudes, particularly at higher elevations, where

wave amplitudes are larger. It is interesting that above 90 km, especially above 94 km, the variance of the VVP zonal wind increases at a rate similar to the lidar, and is significantly higher than that of monostatic measurements.

Figure 8c shows the meteor radar/lidar ratio of zonal wind, calculated using the method in Figure 6. The zonal wind ratios of VVP/lidar are similar to MC/lidar below 90 km. However, above 90 km, the VVP/lidar ratios become larger than MC/lidar, with their difference increasing with height. The zonal wind ratios from monostatic measurements show a decreasing trend with height, consistent with previous studies (Qiao et al., 2025). However, the ratio from VVP measurement has a value of 0.82 at 86 km and increases with altitude to 0.93 at 96 km. This altitude-dependent increasing trend contrasts with the decreasing trend of monostatic result.

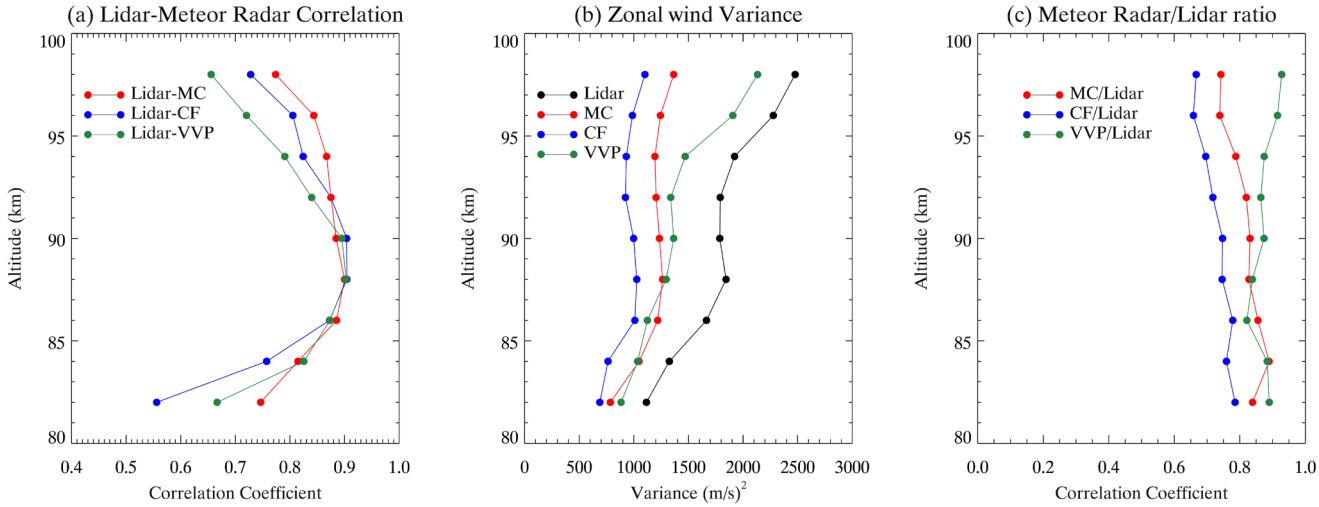

Figure 8. (**a**) Vertical profiles of the correlation coefficient for lidar-MCMR (red line), lidar-CFR (blue line), and lidar-VVP (green line). (**b**) Vertical profiles of zonal wind variance from Na lidar (black line), MCMR (red line), CFR (blue line), and VVP (green line). (**c**) Vertical profiles of zonal wind ratio for MCMR/lidar (red line), CF/lidar (blue line), and VVP/lidar (green line).

We also compared the average zonal wind variation over the night at different altitude. Figure 9 shows the zonal wind variation at 86 km, 88 km, 90 km, and 92 km, respectively. At these altitudes, the average zonal wind varied from -10 m/s to 50 m/s through the night. In Figure 9a, a max eastward wind is 50 m/s occurs at 12:00 UT, while a negative peak of -10 m/s appears at 18:00 UT. The timing of the negative peak is delayed as altitude decreases (16:00 UT at 92 km, 17:00 UT at 90 km and 88 km, and 18:00 UT at 86 km), indicating the presence of a wave with phase speed is approximately 3 km/h, similar to the semidiurnal phase speed in the MLT region. We can also get the vertical wavelength of the semidiurnal, which is 36 km, consistent with previous observations over Hefei (Li et al., 2018). The zonal winds in Figure 9 are modulated by upward-propagating semidiurnal tides. Comparing the zonal winds from the lidar and radars, it is evident that all instruments capture the strong tidal structure, exhibiting very similar phases and amplitudes. The correlation coefficients between 86 and 92 km exceed 0.9, indicating that the Na lidar and meteor radars demonstrate strong consistency and effectively capture

large-scale variations such as tides. It also needs to be noted that the zonal wind variations of lidar are generally larger than those from radars (e. g., 12:00 UT in Figure 9a, 17:00 UT in Figure 9b, and 17:00 UT in Figure 9c), which is consistent with scatter plots result shown in Figure 6.

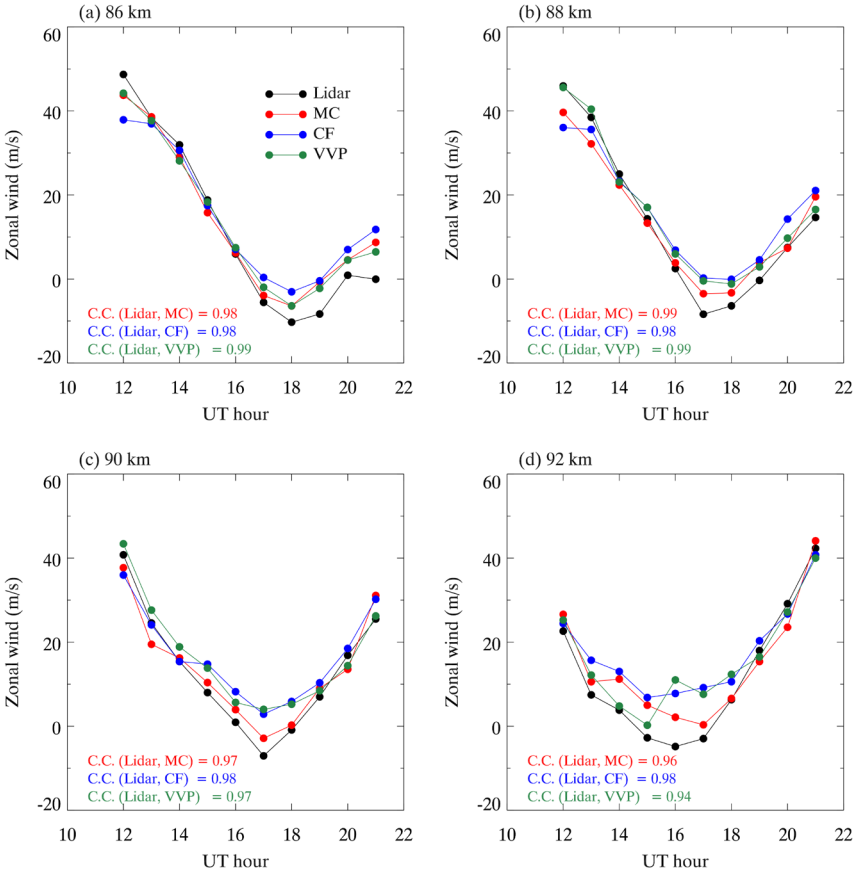

Figure 9. Comparison of Na lidar (black lines), MCMR (red line), CFR (blue lines), and VVP (green lines) zonal wind measurements (**a**) at 86 km, (**b**) at 88 km, (**c**) at 90 km, (**d**) at 92 km averaged at every hour. The correlation coefficients are also presented.

4 Discussion

By comparing the zonal wind measured from Na lidar and meteor radars, we found that the mean zonal wind of lidar and meteor radar showed good consistency. The Na lidar zonal wind speed is larger than that of meteor radars is similar to previous study (Qiao et al., 2025). Interestingly, the zonal wind speed ratios of VVP/lidar, derived from the multistatic meteor radar measurements, are larger than those from the monostatic results (Figure 6). By analyzing the radar/lidar ratios of zonal wind at different altitudes in Figure 8c, we find that the larger VVP/lidar wind ratios mainly arise above 90 km, where the VVP/lidar wind ratios exceed those from monostatic radars. In contrast, below 90 km, the VVP/lidar ratios are

generally consistent with the MCMR results. These results suggest that the VVP method enhances the consistency of meteor radar zonal wind measurements with lidar observations above 90 km.

The vertical profiles of zonal wind variance from the meteor radars and the lidar in Figure 8b also exhibit structures similar to those of the wind speed ratios of radar/lidar. Below 90 km, the VVP zonal wind variance is comparable to that of the MCMR. Above 90 km, however, the VVP zonal wind variance exceeds that of the MCMR and shows a vertical structure similar to the lidar. In particular, above 94 km, the difference in zonal wind variance between the lidar and the MCMR increases progressively. In contrast, the variance from the VVP remains closer to that of the lidar, even showing a decreasing difference, which may explain the increase in the VVP/lidar wind speed ratio between 94 and 98 km in Figure 8c. From both the radar/lidar zonal wind speed ratios and the zonal wind variances, it is evident that the VVP zonal winds are more consistent with the lidar above 90 km.

The observed variations can be partly attributed to differences in the sampling and sensitivity of the two instruments. Meteor detection rates are typically highest between ~85 and 95 km, which provides the most robust wind retrievals (including VVP) because the fitted winds are constrained by the largest number of meteor echoes and the widest distribution of viewing angles. Meanwhile, the Na lidar has its highest signal-to-noise ratio where the sodium number density peaks, which is usually near ~92 km. As a result, as shown in Figure 8a, both instruments have their strongest and most reliable sampling in the overlapping altitude region (~86–94 km), leading to the highest correlation there.

In addition to sampling effects, the improved consistency above ~90 km likely reflects dynamical factors. At these altitudes, wave-driven variability (e.g., tides and gravity-wave-induced perturbations) generally becomes stronger, producing larger-amplitude wind fluctuations. Such larger signals are more readily captured by both instruments despite their different sampling strategies and effective resolutions, which can further enhance the apparent agreement. We therefore interpret the better correspondence above ~90 km as resulting from a combination of (i) optimal overlapping sensitivity and sampling and (ii) larger-amplitude dynamics in the upper MLT that are robustly detected by both radar and lidar.

There is also a noticeable difference in the variance between the MCMR and CFR. As shown in Figure 8b, the difference is approximately 200 m^2/s^2. The variance difference may be caused by the difference of wind average region from MCMR and CFR. The MCMR captures backscatter signals from a circular area with approximately 200 km radius, where meteors are predominantly concentrated between 60 and 160 km (Figure 1b). In contrast, the CFR employs a forward scattering technique, receiving signals from meteors distributed in a circular area with a 300 km radius (Figure 1c), which is broader than that of MCMR. In the same time, the CFR meteor echoes are primarily distributed between 60-220 km (Figure 1c), which is more evenly than MRMC. The more widely and evenly averaging area of the CFR may result in more waves being averaged, leading to a smaller zonal wind variance measured by the CFR. A further comparison among the lidar, meteor radar, and VVP zonal winds variance shows the relationship lidar > VVP > MCMR > CFR. The radius of the corresponding horizontal averaging scales for the lidar, VVP, MCMR, and CFR are 0.04 km, 50 km, 220 km, and 300 km, respectively, indicating that larger averaging scales smooth out more fluctuations and thus lead to smaller zonal wind variances, consistent with previous studies (Liu et al., 2002).

To compare our result with reports from other stations, Table 3 summarizes the conclusions of studies including comparison of mesopause zonal wind between Na lidar and meteor radar at Starfire Optical Range, New Mexico (35° N, 106.5° W) (Liu et al., 2002), Maui, Hawaii (20.75° N, 156.43° W) (Frank et al., 2005), ALO (30.25° S, 71.00° W) (Qiao et al., 2025). Generally, the results from all four stations indicate a good consistency between the wind measurements of lidar and radars. For instance, our lidar/radars correlation coefficients for zonal wind and median differences in zonal wind are similar to the results in Frank et al. (2005), with correlation coefficients ranging from 0.8 and 0.9 and median differences of less than 1 m/s. As shown in Table 3, this study employs over 2000 coincident wind pairs, including nearly 300 hours of observations at each altitude between 88 and 92 km, comparable to that reported by Qiao et al. (2025). The lidar/radars differences in this study exhibit a Gaussian distribution, as shown in Figure 7, which varies from the distribution reported by Frank et al. (2005). The mean zonal winds for these three stations are 15.13 m/s (Hefei), 7.3/18.0 m/s (SOR), and -4.4 m/s (Maui), indicating that background winds vary across different regions.

Case	Height Range (km)	Samples number	Mean winds (m/s)	C.C.	Median Difference (m/s)	Lidar Variance (m^2/s^2)	MR Variance (m^2/s^2)	MR scattering type and Sites (Lat, Lon)
This study	82-98	2216	15.13 (14.25)	0.85	0.52	1857	1192	MC, Backscatter, near Hefei (31.8°N,117°E)
			15.13 (15.96)	0.82	-0.73		951	CF, Forward scatter, near Hefei (31.8°N,117°E)
			15.13 (15.57)	0.80	-0.13		1398	VVP, Multi-static site, near Hefei (31.8°N,117°E)
Liu et al., (2002)	86, 93	126, 97	7.3 (8.9), 18.0 (12.2)	0.65, 0.70	-1.6, 5.8	756, 1030	580, 1253	Backscatter, Starfire Optical Range (35°N,106.5°W)
Franke et al., (2005)	82-98	326	-4.4 (-3.8)	0.89	-0.2	1308	1217	Backscatter, Maui (20.75°N,156.43°W)
Qiao et al., (2025)	80-105	thousands	——	0.79	——	——	——	Multi-static system, ALO (30.25° S, 71.00° W)

Table 3. Comparison of zonal wind measurements and related parameters from Na lidar and meteor radar at different stations. Note that in the 'Mean Winds' column, the value represents Na lidar (meteor radar) zonal wind.

Table 3 shows that the zonal wind variance of lidar is always larger than that of meteor radar in all three stations, except the variance of SOR at 93 km, which likely due to larger instrumental uncertainties and standard deviation of the meteor radar zonal wind at SOR (Liu et al., 2002). This disparity between Na lidar and meteor radar is primarily attributed to the different averaging regions of the two techniques: the meteor radar averages over a circular region with a 200 km radius,

while the Na lidar measures wind within a much smaller area of about 80 m. Specifically, the lidar zonal wind variance in this study is 1857 m^2/s^2, which is larger than that of SOR (756 m^2/s^2 at 86 km and 1030 m^2/s^2 at 93 km) and Maui (1308 m^2/s^2). Although the time resolution of the data from all three stations is uniformly 1 hour, the vertical resolution used in this study is 2 km, smaller than that of SOR (4 km for 86 km, 6 km for 93 km) and Maui (4 km). This higher vertical resolution enables the USTC Na lidar to detect shorter vertical wavelength waves, which may lead to larger wind perturbations and increased wind variance.

In addition to Na lidar and meteor radar, middle frequency (MF) radar and Fabry–Pérot interferometer (FPI) are ground-based methods for measuring wind in the mesopause region. Reid et al. (2018) compared the wind measured by 33.2 (55) MHz MR and 1.98 MHz MF radar at Davis station, finding that the MF radar zonal wind is 0.38–0.95 (0.41–0.85) times that of MR at different altitudes. Similarly, Cervera and Reid (1995) reported a slope of 0.38 and 0.80 for MF and MR below and above 90 km at Buckland Park. The studies indicate that the zonal wind from MR is generally larger than that of MF radar. Recently, Gu et al. (2021) compared wind from MR and FPI at Kunming, finding a slope of ~1.3, which aligns with a comparison study conducted in the Antarctic Peninsula (Lee et al., 2021). The comparison studies between MR and FPI revealed that the zonal wind measured by MR is generally greater than that measured by FPI. Additionally, the comparison of wind measurements between Na lidar and MR in this study and that of Qiao et al. (2025) indicates that the wind measured by Na lidar is generally larger than that from MR. These comparisons suggest that among the four commonly used methods for detecting wind in the mesopause region, the wind measured by lidar is the largest. This may be attributed to lidar's ability to measure wind within a very narrow region (~100 m in diameter at 80–100 km), allowing it to capture more small-scale fluctuations. In contrast, other instruments, such as meteor radar, are better suited for analyzing large-scale waves (e.g., tides and planetary waves) because they averaged small-scale fluctuations, are less susceptible to weather effects, and can continuously collect data.

5 Summary

This study compares simultaneously observed zonal winds from a Na lidar and nearby multistatic meteor radar system during 2022-2023. In total, 2216 datasets collected over 34 nights, corresponding to approximately 300 hours of observations, were used to compare zonal winds in the 82–98 km altitude range. The center height of the Na density from Na lidar is 92.29 km in the Hefei area, which is higher than the maximum meteor count height of MCMR and CFR, which are 89.97 km and 91.10 km respectively. The zonal winds and differences in zonal wind from Na lidar and meteor radars follow Gaussian distributions. The similar mean zonal wind, small mean difference (less than 1 m/s), and high correlation (larger than 0.8) between lidar and radar, indicate that the zonal wind measurements from the Na lidar and multistatic meteor radar system are generally consistent.

The zonal wind speed measured by Na lidar is approximately 1.25 times of MCMR, 1.39 times of CFR, and 1.15 times of VVP. Combine previous comparative studies involving Na lidar, meteor radar, MF radar, and FPI, we conclude that even

using the same temporal resolution and vertical resolution, Na lidar provides the largest wind measurements among these four commonly used ground-based detection instruments. The zonal wind variances from the Na lidar and meteor radars (Table 1) show that Na lidar exhibits a larger variance than meteor radars. This trend is consistent across lidar and radar data variances at all altitudes. This characteristic of zonal wind variance is mainly due to the different horizontal averaging scales of the datasets.

With the Na lidar zonal winds as a reference, the VVP zonal wind variances show better agreement with the lidar than those from monostatic meteor radars (MCMR and CFR), especially above 90 km. Similarly, the radar/lidar zonal wind ratios indicate that the VVP wind speed are closer to the lidar values above 90 km. These results suggest that the VVP method can reliably retrieve middle and upper atmospheric zonal winds, providing improvements over monostatic measurements between 90-98 km and making it suitable for future studies of middle and upper atmospheric dynamical processes.

Data availability: The Na lidar and meteor data shown in this work can be downloaded from Science Data Bank repository (https://doi.org/10.57760/sciencedb.15827) and cited as Ban et al., (2025).

Author Contributions: CB wrote the initial draft of the paper with contributions from all authors. CB, FX, PW, and LT contributed to the preparation of the sodium lidar data products. YW, ZJ, and XX contributed to preparation of the meteor radar data products. All authors participated in the scientific discussion and to the review of the paper.

Competing interests: Author Wen Yi is a member of the editorial board of AMT but was not involved in the review process or editorial decision for this manuscript.

Acknowledgements: This work was supported by the National Natural Science Foundation of China grants (42394121, 42174183, 42574213); the Joint Open Fund of Mengcheng National Geophysical Observatory (No. MENGO-202316, MENGO-202407). This research was supported by the International Space Science Institute (ISSI) in Bern, through ISSI International Team project #23–580 “Meteors and phenomena at the boundary between Earth's atmosphere and outer space.”

References

Ban, C., Li, T., Fang, X., Dou, X., and Xiong, J.: Sodium lidar-observed gravity wave breaking followed by an upward propagation of sporadic sodium layer over Hefei, China, J. Geophys. Res.-Space Phys., 120, 7958–7969, https://doi.org/10.1002/2015JA021460, 2015.

Ban, C., Fang, X., Yi, W., et al.: Data of "A Comparative Study of Mesospheric Zonal Wind Observations from Na Lidar and Multistatic Meteor Radars above Hefei, China" [data set], V3, Science Data Bank, https://doi.org/10.57760/sciencedb.15827, 2025.

Bishop, R. L., Larsen, M. F., Hecht, J. H., Liu, A. Z., and Gardner, C. S.: TOMEX: Mesospheric and lower thermospheric diffusivities and instability layers, J. Geophys. Res.-Atmos., 109, A07307, https://doi.org/10.1029/2002JD003079, 2004.

Cao, B., Heale, C. J., Guo, Y., Liu, A. Z., and Snively, J. B.: Observation and modeling of gravity waves propagation through reflection and critical layers above Andes Lidar Observatory at Cerro Pachón, Chile, J. Geophys. Res.-Atmos., 121, 12,737–12,750, https://doi.org/10.1002/2016JD025173, 2016.

Cervera, M. A. and Reid, I. M.: Comparison of simultaneous wind measurements using colocated VHF meteor radar and MF spaced antenna radar systems, Radio Sci., 30, 1245–1261, https://doi.org/10.1029/95RS00644, 1995.

Chau, J. L., Stober, G., Hall, C. M., Tsutsumi, M., Laskar, F. I., and Hoffmann, P.: Polar mesospheric horizontal divergence and relative vorticity measurements using multiple specular meteor radars, Radio Sci., 52, 811–828, https://doi.org/10.1002/2016RS006225, 2017.

Chu, X., Gardner, C. S., Li, X., and Lin, C. Y.-T.: Vertical transport of sensible heat and meteoric Na by the complete temporal spectrum of gravity waves in the MLT above McMurdo (77.84° S, 166.67° E), Antarctica, J. Geophys. Res.-Atmos., 127, e2021JD035728, https://doi.org/10.1029/2021JD035728, 2022.

Franke, S. J., Chu, X., Liu, A. Z., and Hocking, W. K.: Comparison of meteor radar and Na Doppler lidar measurements of winds in the mesopause region above Maui, Hawaii, J. Geophys. Res.-Atmos., 110, D09S02, https://doi.org/10.1029/2003JD004486, 2005.

Fritts, D. C. and Alexander, M. J.: Gravity wave dynamics and effects in the middle atmosphere, Rev. Geophys., 41, 1003, https://doi.org/10.1029/2001RG000106, 2003.

Gardner, C. S. and Liu, A. Z.: Seasonal variations of the vertical fluxes of heat and horizontal momentum in the mesopause region at Starfire Optical Range, New Mexico, J. Geophys. Res.-Atmos., 112, D09113, https://doi.org/10.1029/2005JD006179, 2007.

Gu, S., Hou, X., Li, N., Yi, W., Ding, Z., Chen, J., Hu, G., and Dou, X.: First comparative analysis of the simultaneous horizontal wind observations by collocated meteor radar and FPI at low latitude through 892.0-nm airglow emission, Remote Sens., 13, 4337, https://doi.org/10.3390/rs13214337, 2021.

Guo, Y., Liu, A. Z., and Gardner, C. S.: First Na lidar measurements of turbulence heat flux, thermal diffusivity, and energy dissipation rate in the mesopause region, Geophys. Res. Lett., 44, 5782–5790, https://doi.org/10.1002/2017GL073807, 2017.

Hindley, N. P., Mitchell, N. J., Cobbett, N., Smith, A. K., Fritts, D. C., Janches, D., et al.: Radar observations of winds, waves and tides in the mesosphere and lower thermosphere over South Georgia Island (54° S, 36° W) and comparison with WACCM simulations, Atmos. Chem. Phys., 22, 9435–9459, https://doi.org/10.5194/acp-22-9435-2022, 2022.

Hocking, W. K., Fuller, B., and Vandepeer, B.: Real-time determination of meteor-related parameters utilizing modern digital technology, J. Atmos. Sol.-Terr. Phys., 63, 155–169, https://doi.org/10.1016/S1364-6826(00)00138-3, 2001.

Holdsworth, D. A., Reid, I. M., and Cervera, M. A.: Buckland Park all-sky interferometric meteor radar, Radio Science, 39, RS5009, https://doi.org/10.1029/2003RS003014, 2004.

Hu, X., Liu, A. Z., Gardner, C. S., and Swenson, G. R.: Characteristics of quasi-monochromatic gravity waves observed with Na lidar in the mesopause region at Starfire Optical Range, NM, Geophys. Res. Lett., 29, 2169, https://doi.org/10.1029/2002GL014975, 2002.

Kishore Kumar, G. and Hocking, W. K.: Climatology of northern polar latitude MLT dynamics: Mean winds and tides, Ann. Geophys., 28, 1859–1876, https://doi.org/10.5194/angeo-28-1859-2010, 2010.

Lee, C., Jee, G., Kam, H., Wu, Q., Ham, Y. B., Kim, Y. H., and Kim, J. H.: A comparison of Fabry–Perot Interferometer and meteor radar wind measurements near the polar mesopause region, J. Geophys. Res.-Space Phys., 126, e2020JA028802, https://doi.org/10.1029/2020JA028802, 2021.

Li, T., Fang, X., Liu, W., Gu, S. Y., and Dou, X. K.: Narrowband sodium lidar for the measurements of mesopause region temperature and wind, Appl. Optics, 51, 5401–5411, https://doi.org/10.1364/AO.51.005401, 2012.

Li, T., Ban, C., Fang, X., Li, J., Wu, Z., Feng, W., Plane, J. M. C., Xiong, J., Marsh, D. R., Mills, M. J., and Dou, X.: Climatology of mesopause region nocturnal temperature, zonal wind and sodium density observed by sodium lidar over Hefei, China (32° N, 117° E), Atmos. Chem. Phys., 18, 11683–11695, https://doi.org/10.5194/acp-18-11683-2018, 2018.

Li, T., Ban, C., Fang, X., Li, F., Cen, Y., Lai, D., et al.: Seasonal variation in gravity wave momentum and heat fluxes in the mesopause region observed by sodium lidar, J. Geophys. Res.-Atmos., 127, e2022JD037558, https://doi.org/10.1029/2022JD037558, 2022.

Liu, A. Z., Hocking, W. K., Franke, S. J., and Thayaparan, T.: Comparison of Na lidar and meteor radar wind measurements at Starfire Optical Range, NM, USA, J. Atmos. Sol.-Terr. Phys., 64, 31–40, https://doi.org/10.1016/S1364-6826(01)00095-5, 2002.

Liu, L., Liu, H., Chen, Y., Le, H., Sun, Y. Y., Ning, B., et al.: Variations of the meteor echo heights at Beijing and Mohe, China, J. Geophys. Res.-Space Phys., 122, 1117–1127, https://doi.org/10.1002/2016JA023448, 2017.

Qiao, Z., Liu, A. Z., Stober, G., Fuentes, J., Vargas, F., Adami, C. L., and Reid, I. M.: Chilean Observation Network De Meteor Radars (CONDOR): multi-static system configuration and wind comparison with co-located lidar, Atmos. Meas. Tech., 18, 1091–1104, https://doi.org/10.5194/amt-18-1091-2025, 2025.

Reid, I. M., McIntosh, D. L., Murphy, D. J., and Vincent, R. A.: Mesospheric radar wind comparisons at high and middle southern latitudes, Earth Planets Space, 70, 84, https://doi.org/10.1186/s40623-018-0861-1, 2018.

She, C. Y. and Yu, J. R.: Simultaneous three-frequency Na lidar measurements of radial wind and temperature in the mesopause region, Geophys. Res. Lett., 21, 1771–1774, https://doi.org/10.1029/94GL01417, 1994.

She, C. Y., Krueger, D. A., and Yuan, T.: Long-term midlatitude mesopause region temperature trend deduced from quarter century (1990–2014) Na lidar observations, Ann. Geophys., 33, 363–369, https://doi.org/10.5194/angeo-33-363-2015, 2015.

She, C. Y., et al.: Tidal perturbations and variability in the mesopause region over Fort Collins, CO (41° N, 105° W): Continuous multi-day temperature and wind lidar observations, Geophys. Res. Lett., 31, L24111, https://doi.org/10.1029/2004GL021165, 2004.

Spargo, A. J., Reid, I. M., and MacKinnon, A. D.: Multistatic meteor radar observations of gravity-wave tidal interaction over southern Australia, Atmospheric Measurement Techniques, 12(9), 4791–4812, https://doi.org/10.5194/amt-12-4791-2019, 2019.

Smith, A. K.: Interactions between the lower, middle and upper atmosphere, Space Sci. Rev., 168, 1–21, https://doi.org/10.1007/s11214-011-9791-y, 2012.

Stober, G. and Chau, J. L.: A multistatic and multifrequency novel approach for specular meteor radars to improve wind measurements in the MLT region: Forward Scatter Specular Meteor Radar, Radio Sci., 50, 431–442, https://doi.org/10.1002/2014RS005591, 2015.

Stober, G., Kozlovsky, A., Liu, A., Qiao, Z., Tsutsumi, M., Hall, C., et al.: Atmospheric tomography using the Nordic Meteor Radar Cluster and Chilean Observation Network De Meteor Radars: Network details and 3D-Var retrieval, Atmos. Meas. Tech., 14, 6509–6532, https://doi.org/10.5194/amt-14-6509-2021, 2021.

Stober, G., Liu, A., Kozlovsky, A., Qiao, Z., Kuchar, A., Jacobi, C., et al.: Meteor radar vertical wind observation biases and mathematical debiasing strategies including the 3DVAR+DIV algorithm, Atmos. Meas. Tech., 15, 5769–5792, https://doi.org/10.5194/amt-15-5769-2022, 2022.

Yang, C., Lai, D., Yi, W., et al.: Observed quasi 16-day wave by meteor radar over 9 years at Mengcheng (33.4° N, 116.5° E) and comparison with the Whole Atmosphere Community Climate Model simulation, Remote Sens., 15, 830, https://doi.org/10.3390/rs15030830, 2023.

Yi, W., Xue, X. H., Reid, I. M., Murphy, D. J., Hall, C. M., Tsutsumi, M., et al.: Climatology of the mesopause relative density using a global distribution of meteor radars, Atmos. Chem. Phys., 19, 7567–7581, https://doi.org/10.5194/acp-19-7567-2019, 2019.

Yi, W., Xue, X. H., Zeng, J., et al.: Observation of MLT region winds and tides by the USTC Mengcheng meteor radar, J. Univ. Sci. Technol. China, 53, 0501, https://doi.org/10.52396/JUSTC-2022-0158, 2023.

Yuan, T., et al.: Seasonal variation of diurnal perturbations in mesopause region temperature, zonal, and meridional winds above Fort Collins, Colorado (40.6° N, 105° W), J. Geophys. Res.-Atmos., 111, D06103, https://doi.org/10.1029/2004JD005486, 2006.

Yuan, T., Heale, C. J., Snively, J. B., Cai, X., Pautet, P.-D., Fish, C., Zhao, Y., Taylor, M. J., Pendleton, W. R. Jr., Wickwar, V., et al.: Evidence of dispersion and refraction of a spectrally broad gravity wave packet in the mesopause region observed by the Na lidar and Mesospheric Temperature Mapper above Logan, Utah, J. Geophys. Res.-Atmos., 121, 579–594, https://doi.org/10.1002/2015JD023685, 2016.

Yue, J., She, C. Y., and Liu, H. L.: Large wind shears and stabilities in the mesopause region observed by Na wind-temperature lidar at midlatitude, J. Geophys. Res.-Space Phys., 115, A10307, https://doi.org/10.1029/2009JA014864, 2010.

Zeng, J., Stober, G., Yi, W., Xue, X., Zhong, W., Reid, I., et al.: Mesosphere/lower thermosphere 3-dimensional spatially resolved winds observed by Chinese multistatic meteor radar network using the newly developed VVP method, J. Geophys. Res.-Atmos., 129, e2023JD040642, https://doi.org/10.1029/2023JD040642, 2024.